

UC Berkeley

UC Berkeley Previously Published Works

Title

Airborne flux measurements of biogenic isoprene over California

Permalink

<https://escholarship.org/uc/item/5v3683x6>

Journal

Atmospheric Chemistry and Physics, 14(19)

ISSN

1680-7316

Authors

Misztal, PK

Karl, T

Weber, R

et al.

Publication Date

2014

DOI

10.5194/acp-14-10631-2014

Copyright Information

This work is made available under the terms of a Creative Commons Attribution License, available at <https://creativecommons.org/licenses/by/4.0/>

Peer reviewed



Airborne flux measurements of biogenic isoprene over California

P. K. Misztal^{1,2}, T. Karl^{2,*}, R. Weber¹, H. H. Jonsson³, A. B. Guenther^{2,**}, and A. H. Goldstein¹

¹University of California at Berkeley, Berkeley, California, USA

²National Center for Atmospheric Research, Boulder, Colorado, USA

³Center for Interdisciplinary Remotely-Piloted Aircraft Studies, Monterey, California, USA

* now at: Institute for Meteorology and Geophysics, University of Innsbruck, Innsbruck, Austria

** now at: Atmospheric Sciences and Global Change Division, Pacific Northwest National Laboratory, Richland, Washington, USA

Correspondence to: P. K. Misztal (pkm@berkeley.edu)

Received: 30 January 2014 – Published in Atmos. Chem. Phys. Discuss.: 24 March 2014

Revised: 31 August 2014 – Accepted: 9 September 2014 – Published: 10 October 2014

Abstract. Biogenic isoprene fluxes were measured onboard the CIRPAS Twin Otter aircraft as part of the California Airborne Biogenic volatile organic compound (BVOC) Emission Research in Natural Ecosystem Transects (CABERNET) campaign during June 2011. The airborne virtual disjunct eddy covariance (AvDEC) approach used measurements from a proton transfer reaction mass spectrometer (PTR-MS) and a wind radome probe to directly determine fluxes of isoprene over 7400 km of flight paths focusing on areas of California predicted to have the largest emissions. The fast Fourier transform (FFT) approach was used to calculate fluxes of isoprene over long transects of more than 15 km, most commonly between 50 and 150 km. The continuous wavelet transformation (CWT) approach was used over the same transects to also calculate instantaneous isoprene fluxes with localization of both frequency and time independent of non-stationarities. Fluxes were generally measured by flying consistently at 400 m ± 50 m (a.g.l.) altitude, and extrapolated to the surface according to the determined flux divergence determined in the racetrack-stacked profiles. The wavelet-derived surface fluxes of isoprene averaged to 2 km spatial resolution showed good correspondence to basal emission factor (BEF) land-cover data sets used to drive BVOC emission models. The surface flux of isoprene was close to zero over Central Valley crops and desert shrublands, but was very high (up to 15 mg m⁻² h⁻¹) above oak woodlands, with clear dependence of emissions on temperature and oak density. Isoprene concentrations of up to 8 ppb were observed at aircraft height on the hottest days and over the dominant source regions.

Even though the isoprene emissions from agricultural crop regions, shrublands, and coniferous forests were extremely low, observations at the Walnut Grove tower south of Sacramento demonstrate that isoprene oxidation products from the high emitting regions in the surrounding oak woodlands accumulate at night in the residual layer above the valley and mix down into the valley in the morning. Thus, the isoprene emissions surrounding the valley have relevance for the regional photochemistry that is not immediately apparent solely from the direct emission flux distribution.

This paper reports the first regional observations of fluxes from specific sources by eddy covariance from an aircraft which can finally constrain statewide isoprene emission inventories used for ozone simulations by state agencies. While previously there was no available means to constrain the biogenic models, our results provide a good understanding of what the major sources of isoprene are in California, their magnitude, and how they are distributed.

This data set on isoprene fluxes will be particularly useful for evaluating potential model alternatives which will be dealt with in a separate paper to assess isoprene emission models and their driving variable data sets.

1 Introduction

Isoprene is the dominant volatile organic compound (VOC) that plays important roles in atmospheric chemistry such as fueling tropospheric ozone production, forming secondary organic aerosols, and acting as an important radical sink

in regions near sources. The global annual source strength of gas-phase biogenic volatile organic compounds (BVOC) is around 1 Pg (10^{15} g) (Guenther et al., 2012). One half of these mass emissions (500 Tg) is constituted by a single highly reactive hemiterpene, isoprene (2-methyl-1,3-butadiene). The other half is represented by hundreds to thousands of compounds which span the atmospheric lifetime ranges from a few seconds (e.g., sesquiterpenes) to months (e.g., benzene), and are actively exchanged in both directions (emission and deposition) between the biosphere and atmosphere (Park et al., 2013). Currently, BVOC measurements (mostly of emission) have been reported at ecosystem scales primarily from fixed tower sites which offer very good temporal resolution, but lack spatial resolution across the broader landscape that is critical for understanding regional photochemistry.

Since the discovery of substantial isoprene emissions from forested regions (Rasmussen, 1970), and subsequent progress in understanding isoprene biochemistry (Loreto and Sharkey, 1990), much research has been conducted to understand the emissions of isoprene and the factors that drive them at the leaf level, including in California (Arey et al., 1991, 1995; Baker et al., 1999; Karlik and Winer, 2001; Kurpius and Goldstein, 2003; Goldstein and Schade, 2000; Schade et al., 1999; Schade et al., 2000; Schade and Goldstein, 2001; Winer et al., 1992). This work has led to BVOC emission models such as the Biogenic Emission Inventory System (BEIS) (Pierce et al., 1998), the Model of Emissions of Gases and Aerosols from Nature (MEGAN) (Guenther et al., 2012) and the Biogenic Emission Inventory Geographic Information System (BEIGIS) (Scott and Benjamin, 2003), which are driven by information about weather conditions, plant distributions, leaf area, and the temperature and light response of isoprene emissions from plants. There have been isoprene flux measurements at the canopy scale in a variety of locations worldwide: northwestern US oak savanna (Lamb et al., 1986), northeastern US mixed forest (Goldstein et al., 1998), northern central US mixed forest (Westberg et al., 2001; Apel et al., 2002), Amazonian tropical forests (Rinne et al., 2002; Kuhn et al., 2002), Central Africa rainforest (Serca et al., 2001), Borneo rainforest (Langford et al., 2010), etc. However, in California, no ecosystem scale fluxes have ever been reported for an oak dominated ecosystem that could be used to verify the modeled statewide isoprene emission inventory.

A California BVOC model called BEIGIS (Scott and Benjamin, 2003) predicts significant emissions of isoprene from oak woodlands distributed throughout the foothills of the Coast Range and the Sierra Nevada mountains (Fig. 1a). However, with the exception of a single site in a pine plantation (Schade et al., 1999; Schade et al., 2000; Goldstein and Schade, 2000; Schade and Goldstein, 2001), and measurements in a few crops (Karl et al., 2008; Fares et al., 2011; Fares et al., 2012; Park et al., 2013), there have been no measurements of BVOC fluxes from California landscapes

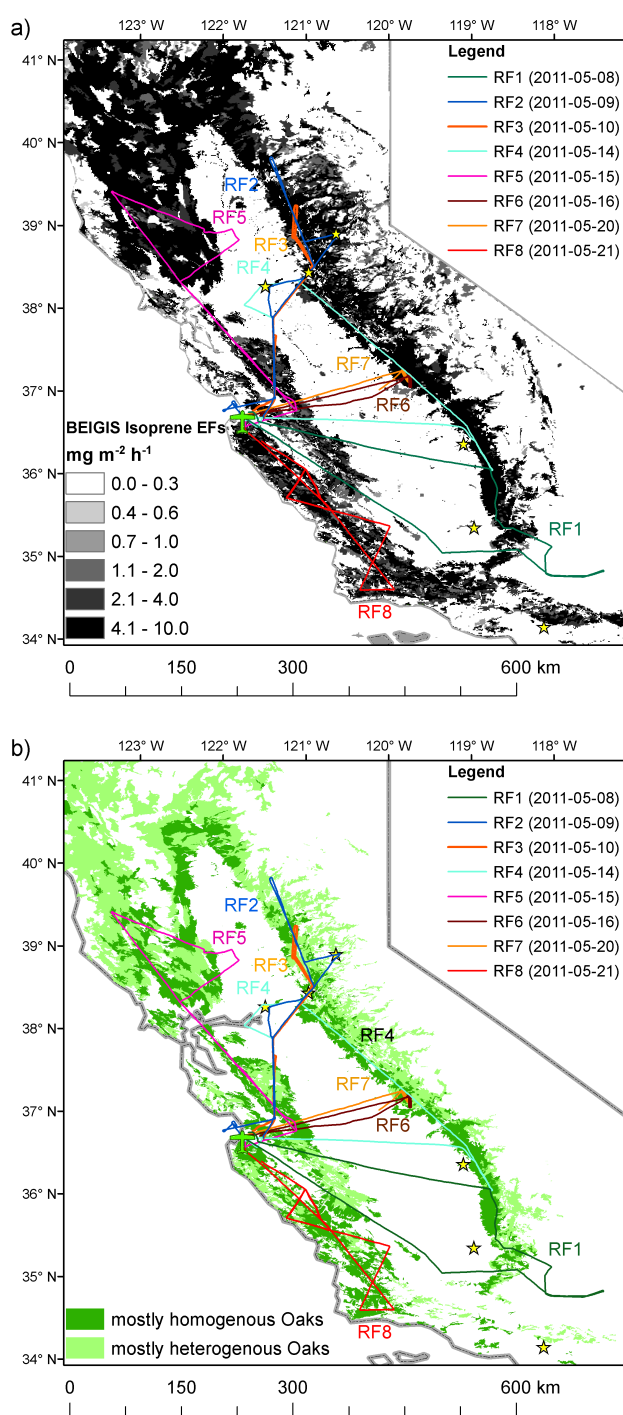


Figure 1. Tracks flown during CABERNET overlaid over (a) BEIGIS-isoprene-emission-factor (EF) land cover; and (b) oak woodland ecosystems differing in oak species spatial homogeneity (according to the GAP database).

at a larger spatial scale than individual leaves and branches. The goal of the CABERNET project was to measure the distribution of isoprene flux across the oak woodland areas of California in order to test and improve the landscape-scale

emission models that are used for regional air quality assessments. The motivation for conducting this regional flux study in California was driven by the following: (1) the need for spatially resolved data on BVOC emissions from oak woodlands which have a large impact on regional ozone concentrations, and (2) our lack of information on how BVOC emissions respond to variations in land cover (plant functional type distributions, leaf area index (LAI), etc).

California is a region where these observations are particularly needed because of its varied landscape, with BVOC emissions from biogenic areas dominated by Oaks ($\sim 7\%$ of land area), and with anthropogenic VOC emissions from the activity of ~ 35 million people living in the state. Furthermore, the accuracy of isoprene emission estimates is important for regional simulations of ozone production.

Airborne eddy covariance (AEC) is an established technique which has been used extensively in the last several decades to measure fluxes (e.g., of energy, ozone, carbon dioxide, etc.) directly using an aircraft (e.g., Lenschow et al., 1981; Desjardins et al., 1992; Pattey et al., 2002; Metzger et al., 2013). The first successful implementation of AEC for VOC was by Karl et al. (2009) over Mexico using a C130 aircraft.

We begin this paper (Sect. 2) by describing the methodology used and the context of the CABERNET airborne campaign including the study region, climatology, flight-track planning, aircraft, instrumentation, and the airborne flux methodologies. We then present results and discussion (Sect. 3) of the isoprene concentration and flux measurements focused on transects over areas expected to dominate BVOC emissions in California. Stacked racetrack profiles which were used for testing the flux methodology and derivation of flux divergence terms were recently described in a separate paper (Karl et al., 2013) where we demonstrated that our proton transfer reaction mass spectrometer (PTR-MS) configuration in CABERNET was appropriate for measuring isoprene fluxes. We quantify and discuss the significance of isoprene emissions from the extensive oak woodlands surrounding the California Central Valley, in which previous studies considering only concentration measurements, and without an accurate understanding of isoprene loss rates and regional dynamics, may have underplayed the role of isoprene for photochemistry in the Valley. Based on simultaneous measurements from a tall tower south of Sacramento, we demonstrate the abundance of isoprene oxidation products is significant regionally even when the abundance of primary isoprene is low. Finally, we report the first observed regional spatial distribution of isoprene airborne fluxes and emission factors and demonstrate that they match well the emission factors from land covers estimated using a California Air Resources Board implementation of the MEGAN model. The comparison of observed fluxes with emissions models will be more thoroughly explored in a separate paper focused on improving land-cover databases and accuracy of isoprene inventories in California (Misztal et al., 2014).

2 Methodology

2.1 Study region

Oaks are the main source of isoprene in California and they grow dominantly in certain elevations (400–800 m) along the foothills encompassing the Central Valley and along the Coastal Range Mountains. These specific locations, relatively constant elevations, and high emission rates make oaks an ideal subject for flux observations from aircraft. Using the USGS (US Geological Survey) National Gap Analysis Program (GAP) land-cover database, we planned our survey flights (to infer surface fluxes from flux measurements over long transects at constant altitude) and race-track flights at several levels (vertical profiles to characterize flux divergence) over more or less homogeneous oak woodlands consisting of the Blue Oak (*Quercus douglasii*) Woodlands (BOW), Valley Oak (*Q. lobata*) Woodlands (VOW) and Coastal Oak (*Q. agrifolia*) Woodlands (COW). The total percentage of the sum of their primary, secondary and tertiary levels was used to map out the most homogeneous areas where oaks are the only or the dominating tree species (see Sect. 2.3 on flight track planning). Despite this biological homogeneity the oaks have highly irregular distribution patterns characterized by varying spatial densities. Supplement Fig. S1 shows a typical oak ecosystem as seen from the Twin Otter flying over Tonzi Ranch tower, where ground flux measurements of isoprene were simultaneously performed for comparison with the aircraft observations (see Sect. 3.2.2). Apart from relatively homogeneous (in terms of the species) oak woodlands mostly in the foothill bands, further away there are transition areas with coniferous regions where, according to the GAP database, the oaks transition into blue oak-ponderosa (BOP) habitats and/or montane hardwood conifer (MHC), and/or montane hardwood (MHW). These areas are represented in Fig. 1b.

2.2 Climatology during field campaign

Environmental context is important to take into account when analyzing measured isoprene fluxes because the history of temperature and photosynthetically active radiation (PAR) is the main driver of potential vegetative emissions (Sharkey et al., 1999; Fuentes and Wang, 1999), and seasonal variability in climate is known to affect gross ecosystem production in this region (Goldstein et al., 2000). The climatological conditions in California in June 2011 were relatively colder than in June of the previous year. The preceding month and the first week of June 2011 were particularly cold followed by gradual increase in the temperature throughout the campaign with particularly hot sunny weather on the final flight of the campaign. Along with the warming, the environment was becoming dryer.

2.3 Flight track planning

The CABERNET airborne campaign took place in June 2011. The paths of the research survey flights and racetrack gradient flights are portrayed over the BEIGIS isoprene emission factor map (Fig. 1a) and California map of oak woodland distribution (Fig. 1b). Weather forecasting was used to ensure that all the flights were conducted on cloudless days, and where possible for the mean wind direction to be perpendicular to the flight paths. A test flight on June 1st was performed over the ocean to calibrate the sensors using pitch and yaw maneuvers, according to Lenschow (1986). These were used for dynamic upwash correction and to test the accuracy of coefficients for wind vector transformations to ensure the vertical wind speed is not affected by aircraft motion. More detailed information on these maneuvers made during CABERNET can be found in Karl et al. (2013).

The true air speed (TAS) was kept as constant as possible on all the flights. For the entire campaign the TAS ranged from around 52 to 67 m s⁻¹ with an average of 58 m s⁻¹, and a standard deviation of 2.3 m s⁻¹. The measured air temperature at aircraft altitude ranged from 19.4 to 25.9 °C (mean: 22.5 °C, SD: 1.28 °C) while the temperature at 2 m above the surface (WRF model) was wider in range (from 10.9 to 34.8 °C) and higher by 3.6 °C average temperature.

The available 40 h of flight time was divided into eight research flights (RFs) which were carried out for approximately 4–5 h each during midday.

Further information specific to each research flight (RF) is summarized in Table 1 and described in the Supplement.

2.4 Aircraft

A two-engine UV-18A Twin Otter (the military version of model Series 300) research aircraft was operated by the Center for Interdisciplinary Remote Piloted Aircraft Study (CIRPAS) of the Naval Postgraduate School out of the airport located in Marina, CA near Monterey, CA. The aircraft is equipped with micrometeorological sensors and is capable of eddy flux measurements (Karl et al., 2013). Air was drawn from a 3-inch (76 mm) isokinetic pipe inlet extending above the nose of the plane, resulting in a flow speed inside the tube of about 10 % of the aircraft speed (~ 60 m s⁻¹). The vertical wind speed in the airplane coordinate system was measured by a five-hole radome probe with 33° half angles at the nose of the aircraft. The vertical wind speed with respect to the earth is obtained from this measured vertical wind speed corrected for airplane motions measured by an inertial reference unit. The measured vertical wind speed is affected by the aircraft movement and flow distortion at the nose, but this affect can be minimized by applying corrections based on the Lenschow maneuvers (Lenschow, 1986). More detailed descriptions of this particular aircraft can be found elsewhere (Hegg et al., 2005; Reid et al., 2001).

The aircraft payload allowed for appropriate instrumentation and between one and three research crew members on board. The list of instrumentation included the following: (1) NCAR's airborne PTR-MS for VOC fluxes (Karl et al., 2009), (2) NCAR's custom-built adsorbent-cartridge automatic sampler for GC-MS VOC speciation and validation of contributions to m/z measured by the PTR-MS, (3) a Picarro (1301 m) 2 Hz methane/CO₂ analyzer, (4) a slow ozone analyzer (2B Tech) and dry chemo-luminescent fast-ozone sensor (NOAA), and (5) a water-based condensation-particle counter (CPC, TSI Inc.).

The VOC cartridge sampler containing eight adsorbent tubes was manually activated during the flight and was recorded by a data-logger analog input to mark the timing of each sample, which was drawn automatically through the cartridge for 8 min at a constant flow of 335 standard cubic centimeters per minute (sccm). In addition, one tube served as a blank for each flight and one tube was kept open inside the cabin for passive absorption of VOCs present in the cabin air to help in the identification of potential tube leaks.

2.5 Proton transfer reaction mass spectrometry (PTR-MS)

The proton transfer reaction mass spectrometer (PTR-MS) can measure concentrations of VOC in a high frequency (10 Hz) virtual disjunct mode (Karl et al., 2002). Unlike a disjunct sampler which rapidly grabs a sample periodically, a PTR-MS instrument can be regarded as a virtual disjunct sampler where the ambient air is sampled continuously but m/z are analyzed sequentially by the quadrupole detector, creating a disjunct data set with high frequency data (e.g., 10 Hz) separated by a relatively longer gap (e.g., 0.5 s). Thus, the 10 Hz disjunct sampling corresponded to 0.1 s dwell time and approximately 2 samples per second.

The instrument deployed in CABERNET was NCAR's high sensitivity PTR-MS (Karl et al., 2009). Its internal vacuum inlet system was specifically redesigned to enable stable operation across a wide range of altitudes and to ensure internal lag time of less than 100 ms. The instrument operation and routine were kept consistently constant for each flight. Current FAA regulations do not allow for the instrumentation to be running overnight, requiring specific steps to achieve stable instrument operation quickly after an instrument starts up. A flight-optimized vacuum system and internal capillary components result in fast transfer time from the inlet to the drift tube and independence of ambient pressure variations on the drift-tube pressure at high altitudes. The valves between the water reservoir and the ion source reduce the time to achieve ion source stability and low oxygen ion levels in the drift tube. Approximately 3 h before the takeoff, the instrument was powered up, and approximately 1 h before the takeoff, if the O₂⁺ signal went below 6 % of the primary ions, a secondary electron multiplier (SEM) and ion source check with optimization was followed by a dynamic

Table 1. Selected flight parameter data specific to each research flight.

	RF1 8 Jun	RF2 9 Jun	RF3 10 Jun	RF4 14 Jun	RF5 15 Jun	RF6 16 Jun	RF7 20 Jun	RF8 21 Jun
Temperature close to the surface (2 m WRF) (°C)								
Mean (median)	20.6 (21.5)	23.1 (23.8)	24.4 (25.3)	27.8 (28.6)	28.5 (29.4)	24.8 (25.4)	29.7 (30.3)	32.5 (33.4)
SD	3.21	3.21	3.46	2.88	3.24	3.96	2.64	3.54
Min	11.3	10.9	11.4	11.7	12.2	11.8	12.1	11.7
Max	25.9	28.0	29.6	32.1	33.8	31.4	34.9	37.2
5th percentile	14.4	17.1	17.7	23.4	22.6	16.8	26.0	27.0
95th percentile	24.6	27.1	28.5	31.1	32.3	29.6	32.4	36.0
Altitude (m a.g.l.)								
Mean (median)	603 (437)	551 (449)	831 (685)	529 (470)	511 (489)	836 (721)	852 (730)	462 (396)
SD	436	309	575	233	193	461	565	210
Min	127	119	126	209	127	55.3	50.0	160
Max	2410	1830	2790	1720	1460	2610	1870	1540
5th percentile	251	266	285	301	278	291	289	268
95th percentile	1670	1300	2090	949	712	1640	1830	887
Convective velocity scale ^a , w^* (m s ⁻¹)								
Mean (median)	4.40 (4.42)	3.56 (3.46)	3.19 (2.94)	3.20 (3.21)	2.61 (2.47)	3.62 (3.61)	3.42 (3.43)	2.86 (2.62)
SD	1.55	0.92	1.19	1.01	0.79	1.12	0.85	1.11
Min	1.18	1.64	1.27	1.18	0.84	1.72	2.2	1.12
Max	8.25	8.69	8.13	5.72	5.11	6.25	4.95	5.87
5th percentile	1.87	2.22	1.54	1.62	1.46	1.99	2.31	1.33
95th percentile	7.01	5.12	5.25	4.67	4.10	5.58	4.82	4.99
Other flight characteristics								
Takeoff time UTC (local/PDT)	17:30 (11:30)	18:15 (12:15)	18:10 (12:10)	18:05 (12:05)	18:00 (12:00)	19:05 (13:05)	19:05 (13:05)	18:55 (12:55)
Touchdown time UTC (local/PDT)	22:20 (16:20)	22:45 (16:45)	22:10 (16:10)	22:35 (16:35)	22:30 (16:30)	0:05 (18:05)	00:30 (18:30)	23:30 (17:30)
Flight focus	Survey	Survey	Survey, Racetrack	Survey	Survey	Racetrack	Racetrack	Survey
Total length (km)	983	908	802	896	875	1020	835	935
PBL height range (km)	0.9–2.8	1.4–1.7	0.8–1.1	0.4–1.9	1.1–1.1	1.6–1.7	1.2–1.2	0.7–1.4
VOC-related m/z measured (10Hz)*	69, 33, 79, 93, 107	69, 71, 33, 81, 137, 87	69, 71, 75, 33	69, 71, 33, 81, 137, 87	69, 71, 33, 81, 137, 45	69, 71, 87	69, 71, 75	69, 71, 33, 137, 87

^a approximated from wavelet heat fluxes (uncorrected) on survey tracks (including only the lowest racetrack levels);

* m/z 21, 32, and 37 were also measured on every flight at 10, 20 and 20 Hz, respectively.

calibration using two VOC standards (Apel–Riemer), one high concentration (available during preflight) containing low-fragmenting compounds for daily sensitivity curves (i.e., benzene (1.11 ppm), toluene (1.07 ppm), xylenes (4.22 ppm), trimethylbenzene (1.94 ppm), dichlorobenzene (2.61 ppm), and trichlorobenzene (1.14 ppm)) diluted with VOC-free air and another low-concentration standard containing isoprene (10.0 ppb) (also available inflight) which was also used as a back-flushing gas during the takeoffs and touchdowns to prevent the exhaust plumes from contaminating the inlet. Zeros were measured using three different sources: Platinum-catalyzed ambient air; ultra-pure compressed air (Air Liquide); ambient air at the top of the saw-tooth sounding well above the planetary boundary layer (PBL) height. The calibrated normalized sensitivities for calibrated VOCs experi-

enced day-to-day variabilities of less than 30%. The average sensitivity for isoprene was 15.1 normalized counts per second per ppbv (ncps ppbv⁻¹) as a sum of m/z 69 (13.4 ncps ppbv⁻¹) and m/z 41 (2.2 ncps ppbv⁻¹). The m/z 41 ion was used to assess the stability of isoprene fragmentation but only m/z 69 was used in the calculation of concentrations. These high sensitivities ensured low detection limits (e.g., < 10 pptv for isoprene at 1 km averaging (~ 17 s)). The primary ion count rates monitored at m/z 21 were around 2.0×10^7 counts per second (cps) ($\pm 20\%$) so the absolute sensitivities were approximately 20 times higher than the normalized sensitivities (i.e., ~ 300 cps ppbv⁻¹ for isoprene). The sensitivities for compounds not present in the standard were approximated for each day from combining sensitivity curves of the daily calibrations with sensitivity

curves from post-campaign calibrations using several different standards at a range of humidities. The accuracy of sensitivities was estimated at $\pm 10\%$ for direct calibration (5 % standard certification +5 % from dilution) and $\pm 30\%$ for the approach combining post-campaign calibrations. The settings, sensitivities and further methodological remarks are included in the Supplement Table S1.

2.6 Airborne eddy covariance (AEC)

The preferred micrometeorological method for measuring trace gas fluxes in the turbulent boundary layer is eddy covariance (EC). This approach is a direct measurement of the fluctuating vertical wind velocity and trace gas concentration. The flux is determined from the mean covariance between vertical wind velocity (w) and concentration (c) fluctuations and can be expressed as

$$F = \overline{w'c'}, \quad (1)$$

where w' is the difference between the instantaneous and mean vertical wind speed and c' is the difference between the instantaneous and mean trace gas concentration. Here we use c' to represent the time average of the product of these two variables. The major components of an EC flux system are: (1) a system that measures vertical wind speed with a fast (typically < 100 ms) response time; (2) an instrument that measures the targeted atmospheric constituent with a fast response time; and (3) a system to receive and store the data (e.g. data logger or computer). Instruments with slower (> 100 ms) response times can be used to measure the flux associated with lower frequencies but may underestimate the total flux depending on the frequency of the transporting eddies. In some cases this may result in an acceptable error while in other cases an attempt can be made to account for the loss of flux due to inadequate sensor response (Moore, 1986; Rowe et al., 2011). One way for estimating high frequency correction involves using another scalar that is measured with a fast response sensor and then estimating the reduction in flux that results if a digital filter is used to simulate response time of the slower instrument.

EC is used extensively to measure sensible and latent heat fluxes, and has recently been used for networks dedicated to quantifying carbon dioxide fluxes from various landscapes (Baldocchi, 2003). Commercial fast response instruments are available for some compounds (e.g., CO_2 , H_2O , CH_4) and others can be constructed for additional chemical species. EC is generally preferred as the most direct flux measurement method which does not require parameterizations. Fluxes of VOC with short lifetimes can be estimated from flux divergence measurements (Lenschow et al., 1980).

Wyngaard and Brost (1984) proposed that the surface fluxes could also be estimated from measurements of vertical concentration profiles in the daytime convective boundary layer (CBL) that lies above the surface layer and can extend up to several km. This method assumes that the mean vertical

gradient of a conserved species in the CBL is determined by the depth of the CBL (z_i), the convective velocity scale (w^*), and the fluxes at the bottom and the top of the CBL. We used vertical profiles of temperature and humidity measured during “saw-tooth soundings” (steep climbs through PBL and part of the free troposphere [e.g., up to 3 km] at a constant angle followed by the similarly steep descent) to directly characterize z_i and measured sensible heat fluxes to quantify w^* . The CBL gradient-flux technique assumes that boundary layer mixing is dominated by convective turbulence and that boundary layer conditions evolve slowly compared to the convective turnover time of about 7 min. The results are not affected by vertically homogeneous horizontal advection or time dependence in the mean concentration and the method can account for entrainment.

A time scale at a fixed point in the PBL can be related to a length scale by multiplying the time scale by the average wind speed, as long as the frozen turbulence hypothesis, known as Taylor’s hypothesis (e.g., Panofsky and Dutton, 1984), is fulfilled. This hypothesis enables approximate conversion from temporal to spatial statistics. Since aircraft can fly an order of magnitude faster than the mean wind, Taylor’s hypothesis is more easily fulfilled, so the length scales can be calculated by multiplying the measured time scale by the true airspeed.

Area source emission was measured using the airborne eddy covariance technique. Eddy covariance was used to directly measure fluxes of predetermined compounds. Because quadrupole systems analyze mass to charge ratios sequentially, only a small number of compounds can be selected for inclusion into the flux mode to keep the disjunct gap relatively small. The number of masses ranged from three to six during eight research flights. As the project was focused on California vegetation and in particular oak woodlands, isoprene (m/z 69) was measured on all eight research flights, MVK+MACR (m/z 71) and methanol (m/z 33) on seven flights. Other VOCs measured on a smaller number of flights included monoterpenes (m/z 81, 137), MBO (m/z 87), acetaldehyde (m/z 45), benzene (m/z 79), toluene (m/z 93), and C8-aromatics (m/z 107). In this manuscript, we focus solely on the isoprene concentration and flux observations. Spatially resolved eddy covariance fluxes were calculated using wavelet analysis (Mauder et al., 2007) along flight tracks through the convective layer. Since the majority of flights were conducted in the lower part of the mixed layer and the upper part of the surface layer (typically 100–200 m deep based on 10 % of the measured PBL depth), we estimate the horizontal spatial resolution based on the blending height (e.g., Claussen, 1990) using the surface layer scaling and the parameterizations for the mixed layer scaling (Karl et al., 2013).

2.6.1 Airborne virtual disjunct eddy covariance (AvDEC)

The difference between a virtual and a conventional disjunct eddy covariance is that sampling flow is continuous, but the data set becomes disjunct, because the quadrupole detector cycles through the m/z sequentially, producing regular gaps between high-frequency data points. For the small number of m/z scanned by the PTR-MS detector, AvDEC measurements are nearly equivalent to continuous AEC. In order to minimize the disjunct error, the number of samples collected per integral scale should significantly exceed one and the effective duration of the sample period should be maximized. This can be achieved by limiting the number of m/z in the duty cycle and keeping the integration time long. We kept the number of VOC-related m/z between 3 and 6 at 0.1 s dwell time. In addition, on each flight, we monitored three control masses: hydronium ions (m/z 21), oxygen ions (m/z 32), and water vapor (m/z 37) at 0.1, 0.05, and 0.05 s, respectively, so the total duty-cycle length varied from 0.5 to 0.8 s between different flights, which resulted in a sampling rate of 1.25 to 2 samples per second.

2.6.2 Fast Fourier transform (FFT)

Fast Fourier transform (FFT) is the conventional method to compute airborne flux. This method provides a single value for a given segment of flight, which limits the spatial resolution. The optimal stretch for flux calculation would be a sufficiently long pass to capture the optimal range of frequency distribution, but not so long that the turbulent structures are affected by diurnal effects. Therefore, resolution finer than 10 km would be challenging and uncertain using the FFT approach. Another challenge in this method is that it is affected by non-stationarities (e.g., related to heterogeneities). However, as an independent method it can be very useful for comparison with fluxes obtained from wavelet analysis (see Sect. 2.6.3).

2.6.3 Continuous wavelet transform (CWT)

Wavelet analysis, originally demonstrated to work with seismological data, has recently become increasingly popular in environmental and biological applications. Examples can be found in the analysis of the turbulent structures (Thomas and Foken, 2005; Mauder et al., 2007; Steiner et al., 2011; Metzger et al., 2013), and analysis of environmental processes at multiple scales (Stoy et al., 2009; Vargas et al., 2010).

The mathematic principle for the one-dimensional wavelet transform of a given signal $f(t)$ can be presented as follows:

$$T_p(a, b) = \int_{-\infty}^{+\infty} f(t) \overline{\Psi_{p,a,b}(t)} dt, \quad (2)$$

where $T_p(a,b)$ are wavelet coefficients and $\Psi_{p,a,b}(t)$ is the wavelet function given by the following:

$$\Psi_{p,a,b} = \frac{1}{a^p} \Psi\left(\frac{t-b}{a}\right), \quad (3)$$

where $\Psi((t-b)/a)$ is termed “the mother wavelet”, of which shape and locations are determined by the scale parameter of the wavelet a and by the translation parameter b . The normalization factor $1/a^p$ preserves the energy of the original mother wavelet (for $p=1$). A general description of wavelet methodology can be found in Torrence and Compo (1998). We used the Morlet mother wavelet, but there are different types of mother wavelets which can be suitable for different applications. For example, the Mexican-hat mother wavelet works well with detection of single events, for example in the analysis of coherent structures of ejections and sweeps from a closed-canopy forest (Steiner et al., 2011). On the other hand, the complex Morlet function wavelet is suited to analysis of variance spectrum (Thomas and Foken, 2007). Nordbo and Katul (2013) looked at periodicities of long-term CO_2 fluxes from soil. They showed that the intrinsic smoothing property of the wavelet produces results that are more easily interpretable, without the need of excessive manipulation of the original signal (e.g., averaging, smoothing, and tapering) or without restrictive assumptions (e.g., periodicity, stationarity).

The CWT method has an advantage over FFT in that it does not require homogeneity or stationarity, and can reconstruct the time domain to provide specific information on where in space/time and on which frequency the flux occurs. The wavelet flux method allows for the reconstruction of both the frequency and time domains of the flux within a straight stretch of the desired length, and therefore can produce instantaneous or discrete fluxes which can be directly compared with model estimates. From the pragmatic point of view, calculation of an entire flight segment (e.g., of 100 km) results in not just a single flux value but delivers spatially resolved fluxes at discrete intervals sometimes informally referred to as instantaneous fluxes. Considering the footprint and wavelet scaling parameters, it is possible for an aircraft flying low at approximately 60 m s^{-1} to provide meaningful spatial flux representation at the 1–2 km resolution needed for investigating landscape heterogeneity in high resolution biogenic emission models, although in principle even shorter intervals could also be resolved. However, the segment to average the CWT fluxes needs to be sufficiently long to capture all the frequency contributions (e.g., of the order of the PBL depth). We determined that for a sufficiently long stretch (e.g., 20–200 km) it is possible to achieve statistically significant discrete wavelet fluxes, on the order of hundreds of meters. To comply with the range of conditions and to ensure statistical significance for the given surface patchiness, the 2 km flux is not just a single value but it is an aggregate of individual wavelet flux values averaged to 2 km. These 2 km fluxes make it flexible to further average spatially to reduce

random error related to high variability at short time scales (see Sect. 2.7), before comparing observations with model emissions. An average of the wavelet fluxes can be compared to the Fourier flux from the same stretch. Given the independent approaches, the agreement between the methods adds to the confidence of the flux estimates and the ratio can be used as an additional measure of data quality. Finally the co-spectra from the two methods can be compared. If no high-frequency attenuation losses exist, the co-spectra should be similar. The wavelet approach can also be used for the correction of the FFT high-frequency spectral attenuation if it is related to tubing effects or factors other than the instrument response (Nordbo and Katul, 2013). More detailed methodology of wavelet analysis used in this work has been presented by Karl et al. (2013) which was a further development from Karl et al. (2009).

2.6.4 Vertical flux

Vertical flux divergence of isoprene is expected to be primarily controlled by its relatively short lifetime and was measured directly using racetracks at multiple altitudes (Karl et al., 2013). It was found to be similarly linear above different oak ecosystems and heterogeneity. We estimated the contribution of the storage term to the isoprene flux divergence to be of the order of 2–5 %, relatively small compared to the storage term in the temperature budget. Fluxes were generally measured by flying consistently at $400 \text{ m} \pm 50 \text{ m}$ (a.g.l.) altitude, which was chosen so that the resulting blending length and flux footprint match the spatial scale of surface patchiness (Mahrt, 2000; Raupach and Finnigan, 1995; Wood and Mason, 1991; Mason, 1988). The flux at the aircraft altitude was typically in the range of 5 % to 30 % smaller than the surface flux depending on the ratio of aircraft altitude to PBL height (z/z_i), and the determined flux divergence linear coefficients were assumed to be relatively constant based on the range of OH concentration estimates for the entire flight track. An alternative method expected to work with similar accuracy would be to use inverse models (Bange et al., 2006). The wavelet coefficients were optimized for the CWT analysis to perform well on stretches between 15 and 200 km with a typical ratio of FFT single flux value to CWT instantaneous flux average of between 1.0 and 1.3.

2.6.5 Flux footprints

The footprint for each flux point was derived using the Weil and Horst (1992) approach and depends on the wind speed, relative altitude to the PBL height, and the convective velocity scale.

Here we use scaling developed for the mixed layer according to the following:

$$dx_{0.5} = 0.9 \frac{u \cdot z_m^{2/3} \cdot h^{1/3}}{w^*}, \quad (4)$$

where $dx_{0.5}$ is the half width of the horizontal footprint, u the horizontal windspeed, z_m the height above ground, h the PBL height and w^* the convective velocity scale which is derived from the wavelet heat flux in each transect.

The source contribution area can be approximated by projecting an upwind-pointed half dome with the $dx_{0.5}$ parameter representing a radius of that half dome (see Supplement Fig. S5).

2.7 Error analysis (quality of fluxes)

As with eddy covariance on the ground, AEC fluxes must undergo a rigorous quality assessment, if not more so. The total uncertainty in reported airborne flux for a typical flight segment ($> 20 \text{ km}$) is the summation of errors from calculation of concentrations (10 % for calibrated compounds [5 % standard accuracy + 5 % dilution system], 30 % from relative lab-based sensitivity-relative transmission approach), survey-flight-specific random (15 % for the typical leg), systematic (1 %) errors related to relative altitude within the PBL and to the aircraft leg, random error related to disjunct measurement (less than 1 %), error due to storage term (2 %) and error due to variability in flux divergence coefficients ($\sim 2 \%$, explained further below). For reactive tracers which require divergence corrections to yield the surface flux, uncertainty in PBL estimation (interpolated from sawtooth soundings) is $\pm 100 \text{ m}$ which translates to 10 % of up to 30 % of the divergence correction, thus $\sim 3 \%$. We estimate the total accuracy for the reported surface fluxes averaged for long segments (e.g., 100 km) to be 30 % for calibrated compounds and 50 % for other compounds and a typical isoprene flux detection limit of $0.01 \text{ mg m}^{-2} \text{ h}^{-1}$.

The vertical flux divergence is dependent on the rate of isoprene oxidation (which depends mostly on OH concentration during daytime), the time rate of change of isoprene concentration (relevant also for conserved species), and differential horizontal advection of isoprene with height (small). Based on directly measured flux divergence in the race-track gradient flights (Karl et al., 2013) we showed clear linear dependence of the flux divergence with a theoretical vertical concentration gradient (e.g., $1.4 \times 10^{-4} \text{ ppbv m}^{-1}$ over a homogenous oak terrain and an OH concentration of $6.6 \times 10^6 \text{ molec cm}^{-3}$). Since the flux divergence for isoprene was shown to be primarily controlled by OH concentrations (of which we have a range of estimates), we make an informed assumption here that the divergence coefficients we used to scale the fluxes to the surface are accurate within a factor of 2 for the entire campaign. Thus, a change in the flux divergence coefficients by a factor of 2 could result in only a $\sim 2 \%$ difference to the scaled surface flux for a typical z/z_i ratio of 0.3 which is minor relative to other error sources as discussed above. As the correction of the fluxes for flux divergence was typically less than 20 %, the contribution from less accurate divergence coefficients is assumed to be relatively minor (up to $\sim 2 \%$) for isoprene.

The uncertainty of the instantaneous CWT fluxes aggregated to 2 km is dominated by the random error which must be necessarily larger than that for the average flux for the whole leg and is related to high temporal and spatial variability (e.g., Mann and Lenschow, 1994). Using equation 3 from Karl et al. (2013) this error can be of the order of 40–50 % but declines with averaging of the 2 km points and is already below 30 % when averaging more than 5 km. For this reason we have only evaluated fluxes over longer stretches (> 2 km). The 2 km representations can provide more flexibility for averaging, for example, individual points can be useful for a regression of isoprene flux versus LAI for all of the 2 km data providing excellent statistics. However, it makes sense to use spatially averaged data (e.g., regional zones) for comparison with the models. While the footprint averaged data are not shown here, such data would be additionally associated with the error related to footprint accuracy which is related to uncertainty in short-term convective scale velocity, PBL height and any variability in wind speed. Thus, the total uncertainty of the surface fluxes of isoprene is estimated at approximately 50 % for individual 2 km data points, but at 20 % for averages exceeding 10 km.

The calibrated concentration data filtered for interferences (e.g., a biomass-burning episode; see video in the Supplement) were used with corrected vertical wind-speed data to derive covariance functions for each eligible stretch. The segments were selected for flux calculation based on minimal roll angle of the aircraft between turns, and on consistency of altitude, excluding maneuvers with significant altitude changes such as soundings (see example in Supplement Fig. S2). Of segments prescreened for validity, only those with a clear peak in the covariance function (Fig. 2a) within the lag-time window of 5 s were accepted. The segment data were subsequently examined for similarities in the variances of concentration and vertical wind speed (Fig. 2b) together with the time series of wavelet frequency co-spectra (Fig. 2c) within the cone of influence (COI) which is the region where the end of the power spectrum may be impacted by edge effects. Rather than excluding the part falling outside the COI, each of the ends of the time series are padded with zeros and excluded afterward, so the results are not affected by the COI. By comparing the wavelet co-spectra with average cross-covariance (Fig. 2d) it is possible to determine where in the wavelet period (inverse of frequency) the flux contribution occurs, enabling for example the visualization of the updrafts associated with high emissions.

Each stretch was finally analyzed for spectral characteristics, independently for the FFT and CWT methods (see Fig. 3). Identical procedures were applied to the fast temperature sensor for comparison. As the co-spectra and ogives demonstrate, the VOC sampling system was not limited by high frequency attenuation owing to the short 0.1 s dwell time and small number of preselected VOCs in the quadrupole mass spectrometer cycle. It was found that the majority of the flux contribution ($\sim 90\%$) was occurring be-

tween 0.1 and 0.01 Hz which translates to the spatial scales of 0.6 to 6 km.

Additional quality measures were the ratio of the FFT and CWT fluxes (Fig. 4, upper panel), which for isoprene were usually $1 \pm 15\%$ for survey transect flights. Identical values from the two methods were not expected as the FFT flux is affected by nonstationarities and inhomogeneities in contrast to the CWT flux, but the generally good agreement adds confidence to the results. Occasionally, a ratio higher than 1.15 was seen on short segments, or over a nonhomogeneous transect, or when the fluxes were close to zero. In sporadic cases when the fluxes were strongly non-stationary (characterized by the ratio higher than 1.3), the FFT flux was tagged as rejected and the CWT flux was only accepted if all the other quality criteria were fulfilled.

The generally good quality of fluxes in CABERNET was due to a combination of factors such as instrument sensitivities, response times, slow aircraft speeds and proximity to the source by flying at low altitudes (e.g., 400 m) and finally lack of spectral interferences (e.g., from propellers). Figure 4 (lower panel) shows the application of flux divergence (only reactive compounds such as isoprene) coefficients from race-track profiling to derive the surface fluxes from the aircraft fluxes. In the remainder of the manuscript when discussing fluxes, we focus exclusively on the CWT fluxes due to the much higher spatial resolution of the flux and also because of their higher accuracy in cases with inhomogeneity and non-stationarity.

2.7.1 Simultaneous ground-based measurements

Ground-based measurements coinciding with aircraft passes in time and space were performed at two sites: The 525 m tall Hearst-Argyle Tower in Walnut Grove, California (WGC) located in the San Joaquin Delta region south of Sacramento (38.2636, -121.4899 , elevation 1 m) and the 23 m tall Tonzi Ranch tower (TRT) (38.4308, -120.9656 , elevation 177 m) located in the relatively homogenous oak forest savannah below the Sierra Nevada foothills to the east of the San Joaquin Delta. Description of these measurements is provided in the Supplement.

3 Results and discussion

3.1 Observed concentrations of isoprene from PTR-MS

The spatial distributions of isoprene concentrations measured on all research flights are shown in Fig. 5.

Isoprene concentrations were low, typically less than 50 ppt ($0.05 \text{ mg m}^{-2} \text{ h}^{-1}$ in fluxes) in the Central Valley at flight altitude over agricultural terrains and over urban areas, but were very high over the oak woodlands, which cover approximately 7 % of California, and were the focus of the CABERNET campaign flight plans. In general, observed isoprene concentrations over oak woodlands ranged from less

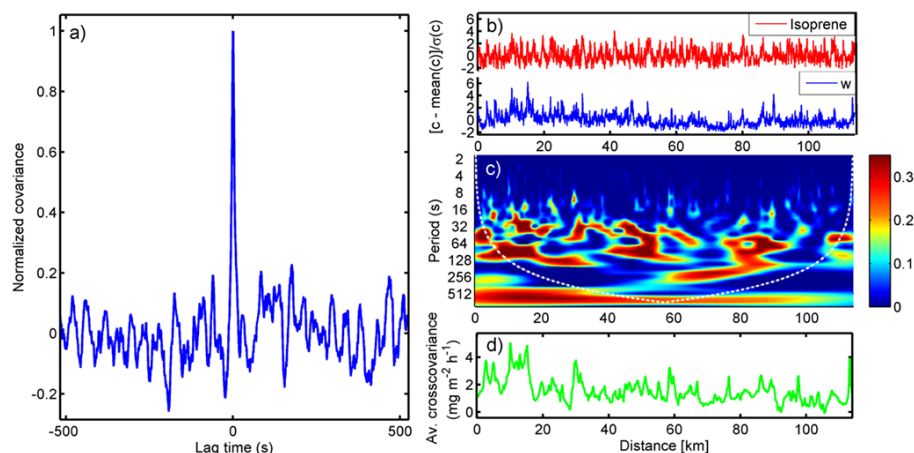


Figure 2. Flux quality control for an example flight leg (the segment from Supplement Fig. S2). (a) Clear peak in the covariance function, (b) variances of vertical wind speed (w) and isoprene, (c) time-resolved wavelet co-spectra, and (d) average cross-variance.

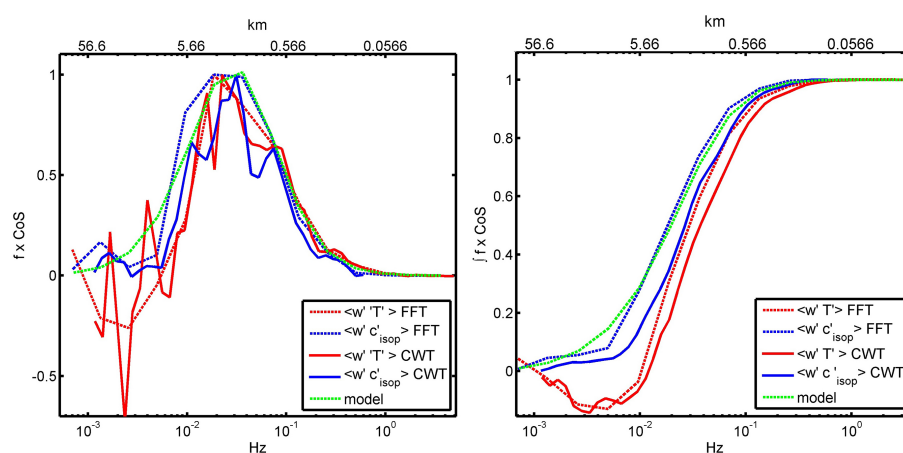


Figure 3. Spectral quality control of the example flight segment. Left panel: comparison of co-spectra for isoprene flux and heat flux using the FFT and CWT methods independently; Right panel: cumulative co-spectra for isoprene flux and heat flux using the FFT and CWT methods independently. The green lines in left and right panels show the model that is used with transfer functions optimized from Kristensen et al. (1997).

than 1 ppb on cool days up to several ppb on warmer flights. A maximum of 8 ppb was observed on the hottest day. The aircraft also saw marked increases of isoprene near some highways with eucalyptus trees planted alongside. Although no study of regional scale emissions of VOC in California was previously conducted, the pattern of concentrations observed during CABERNET is consistent with an expected pattern based on extrapolation of earlier studies from enclosures of dominant plant species of California which suggested oaks (mostly blue oaks), and to some degree eucalyptus trees, to be likely the most important isoprene emitters in California (e.g., Karlik and Winer, 2001). The broad range of temperatures encountered in different flights (mean range 21–33 °C) was responsible for quantitative differences in concentrations over the overlapping segments. The actual concentration at the surface can be significantly higher than ob-

served at aircraft height, as is shown to be the case when flying near the tall tower at Walnut Grove where the top levels (394 and 525 m) saw very tiny concentration of isoprene consistent with the concentrations seen by aircraft although the lowest tower levels (10 and 131 m) saw much higher concentrations (Fig. 6). However, the areas with significant biogenic emissions of isoprene covered a relatively small fetch within the footprint of the Walnut Grove tower.

The Twin Otter flew close to the WGC tower on RF2 and RF4 (13:18). The WGC region is mostly agricultural with a variety of sparsely distributed trees. The measurement during the aircraft pass at 13:18 showed very little isoprene (below 50 ppt) in excellent agreement with simultaneous observations at the top level (525 m) of the tower, even though concentrations around 1 ppb were observed at the 10 m level.

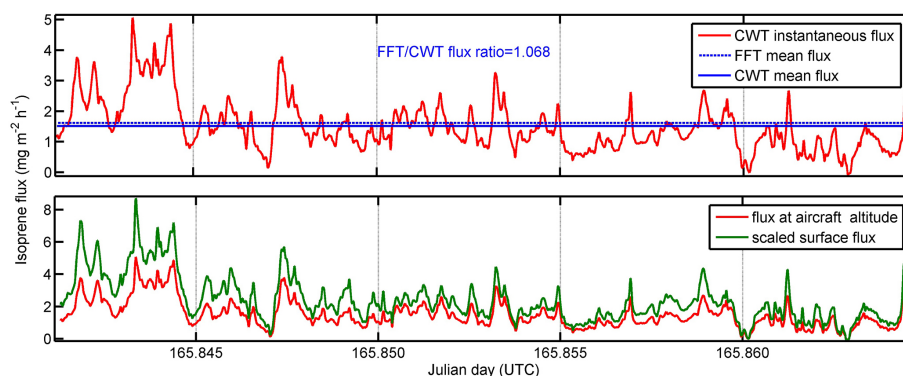


Figure 4. Isoprene flux processing. Upper panel: determination of the FFT/CWT flux ratio; lower panel: application of flux divergence coefficients (derived in racetrack profiles) to scale fluxes from aircraft altitude to surface fluxes using aircraft altitude and PBL height.

3.2 Observed fluxes of isoprene from PTR-MS

In this paper we focus on reporting isoprene surface fluxes.

The observed surface emission rates of isoprene over oak woodlands ranged from around 1 to 15 $\text{mg m}^{-2} \text{h}^{-1}$. The measured isoprene flux distribution shown in Fig. 7 (CWT fluxes, 2 km resolution) visually confirms earlier predictions that isoprene emissions are almost exclusively produced by oak with a limited contribution from eucalyptus trees. For example, when entering the Sierra Nevada foothill oak band, isoprene emissions rose remarkably above the low background ($0\text{--}0.05 \text{ mg m}^{-2} \text{h}^{-1}$) in the Central Valley of California. The fact that isoprene is low over the Central Valley in midday at aircraft altitude does not necessarily mean that regional isoprene emissions are not important for photochemistry in the Central Valley. Isoprene produced by the oaks surrounding the Central Valley gets oxidized during the daytime and its oxidation products such as MVK and MACR can be transported and then may be important for photochemistry when reacting in the presence of anthropogenic pollutants such as NO_x leading to regional ozone and secondary organic aerosol (SOA) formation. Figure 6 demonstrates the case within the Central Valley, where local vegetation is patchy and sparse so isoprene concentration is very low at the aircraft altitude during midday, even though isoprene is observed to be much more abundant near the surface, and in the later afternoon. When the aircraft was passing the tower both the tower's top two inlet levels and the aircraft observed very low but non-zero concentrations of isoprene and MVK+MAC. However, the tower data demonstrate that oxidation products of isoprene routinely accumulate at night in the residual layer due to transport from the surrounding foothills where emissions are high. These high concentrations of isoprene oxidation products above the inversion layer are vented down in the morning when enough surface heating has occurred to cause vertical convection (Fig. 6). Thus, previous studies inferring low significance of isoprene in the Central Valley might not account for this influence of iso-

prene emission from the surrounding foothills in the nighttime residual layer and in the morning when it is mixed vertically, and could therefore likely underplay the role of its oxidation products for regional photochemistry. Thus, to quantify the isoprene emission rates the daytime aircraft flux data are critical, but to understand the impact of isoprene emission in the Central Valley, a combination of the tower and aircraft observations are more useful than the daytime aircraft measurements alone. The extensive oak savannas are strong sources of isoprene. They grow with different area fraction cover and LAI and their regional characterization is crucial for understanding the magnitudes and extent to which these ecosystems contribute to the regional fluxes and the resulting distribution of oxidation products and photochemistry.

Karlik and McKay (2002) used an isoprene emission factor from branch enclosure for blue oak of $27 \mu\text{g g}^{-1} \text{h}^{-1}$, and leaf areas and weights from 14 blue oak trees from Sierra Nevada to estimate a leaf-level emission factor of $\sim 8 \text{ mg m}^{-2}(\text{leaf}) \text{h}^{-1}$, corresponding to a landscape emission factor of $\sim 4 \text{ mg m}^{-2}(\text{land}) \text{h}^{-1}$ for a setting where oaks occupied half of the land surface area. In CABERNET the airborne emission factors for isoprene over oak woodlands varied from less than 1 to $\sim 10 \text{ mg m}^{-2} \text{h}^{-1}$ with the average EF comprising all the flights over areas with oak presence ($\geq 20\%$ coverage of oak species according to GAP database) of $1.8 \text{ mg m}^{-2} \text{h}^{-1}$. However, the woodlands varied in species homogeneity, and more significantly, in the fraction (i.e., sparseness and patchiness) of tree coverage. It is necessary to emphasize that while the LAI of oak covered land surfaces has a relatively small range, about 3 to $6 \text{ m}^2 \text{m}^{-2}$, the fraction of the land surface covered by oaks can range from <0.1 to 1. For example, Karlik and McKay (2002) using a precise method of calculating the areas of leaves from 14 trees divided by the areas of their crowns, measured an LAI of $4.3 \text{ m}^2 \text{m}^{-2}$ for oak crown areas but the oaks only covered 42% of the land surface resulting in an area average LAI of $1.8 \text{ m}^2 \text{m}^{-2}$. For the more sparse terrains the area average LAI can often be lower than $1 \text{ m}^2 \text{m}^{-2}$.

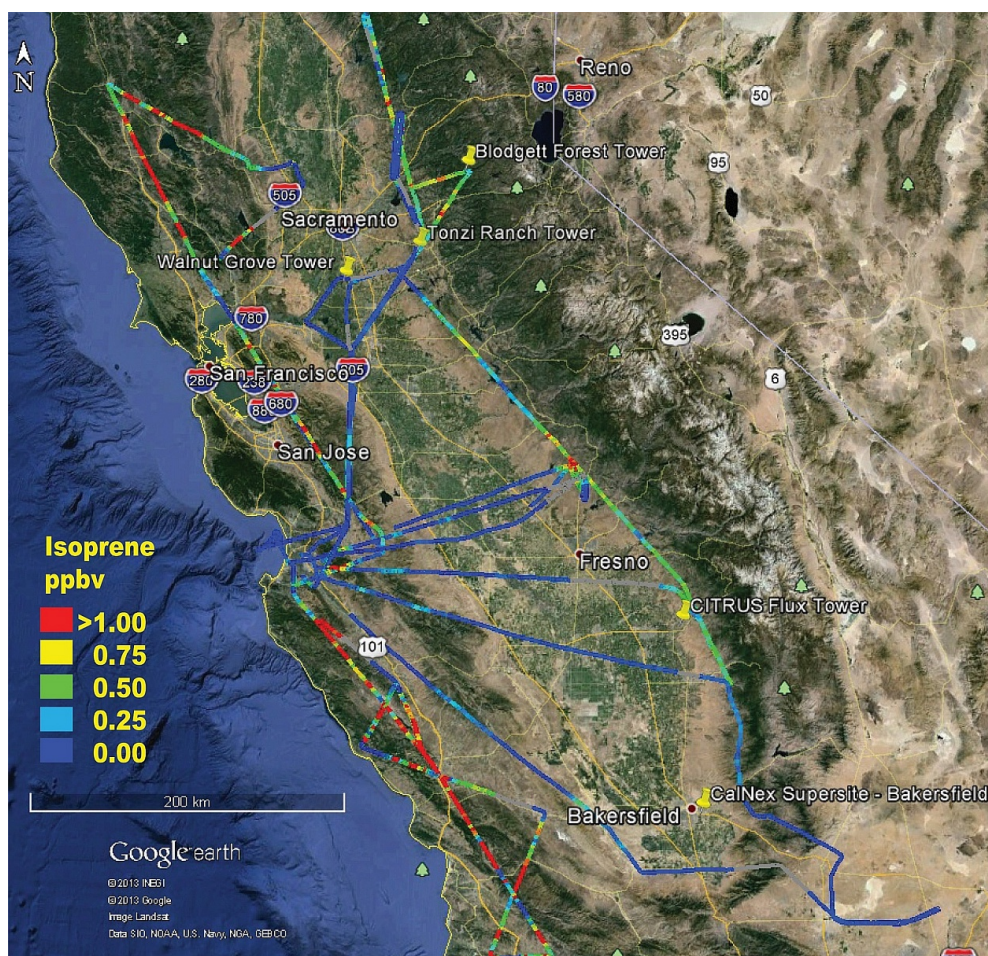


Figure 5. Spatial distributions of isoprene concentrations measured during CABERNET.

Compared with the forests with closed canopies, modeling emissions from oak woodlands in California can be regarded as a specific case to which assessment by airborne flux measurements are particularly applicable. Measured airborne emissions reflect the true emissions from these California ecosystems of variable LAI ranging from less than 1 to about $5 \text{ m}^2 \text{ m}^{-2}$.

Particularly strong isoprene emission hot spots were observed from the dense savannahs on the Sierra Nevada foothills dominated by Blue Oaks where ecosystem BEFs often exceeded $4 \text{ mg m}^{-2} \text{ h}^{-1}$. This oak band is continuous over approx. 800 km starting on the NE side of the valley from above Redding down through the east of Bakersfield and then tapers off before Lancaster. Going east towards the Sierras, for example towards the long-term Blodgett measurement site (Goldstein et al., 2000), the emission factors degrade to around $1 \text{ mg m}^{-2} \text{ h}^{-1}$ or less as the ecosystem becomes conifer-dominated with only some oak trees remaining. Less homogenous isoprene source distribution were observed on the other side of the Central Valley near the coast and at the foothills and above Pacific Coast Ranges Moun-

tains. Although Geron et al. (2001) found that blue oaks, coastal oaks and valley oaks have similar leaf level emission factors (within about 15%), these aircraft measurements indicate that regions where blue oaks mix with coastal oaks and valley oaks have higher isoprene emissions with observed ecosystem BEFs approaching $10 \text{ mg m}^{-2} \text{ h}^{-1}$. As the wind blows from the coast it brings oxidation products to the urban areas in the Central Valley as well as the San Francisco Bay Area. In terms of the air quality of those regions, attention is generally focused on vehicle traffic and other anthropogenic emissions and society is mostly unaware of how important the oak-derived secondary products may be in secondary ozone formation which is driven by a combination of BVOCs and fossil-fuel emissions (Steiner et al., 2006). Until now, data on isoprene emissions in these regions have been completely unavailable, and our airborne measurements clearly show where the emission hot spots are, as well as what magnitudes of isoprene emissions are occurring in these regions close to highly populated cities of California. The distribution of emissions observed near these populated regions with serious air quality problems will be critical for

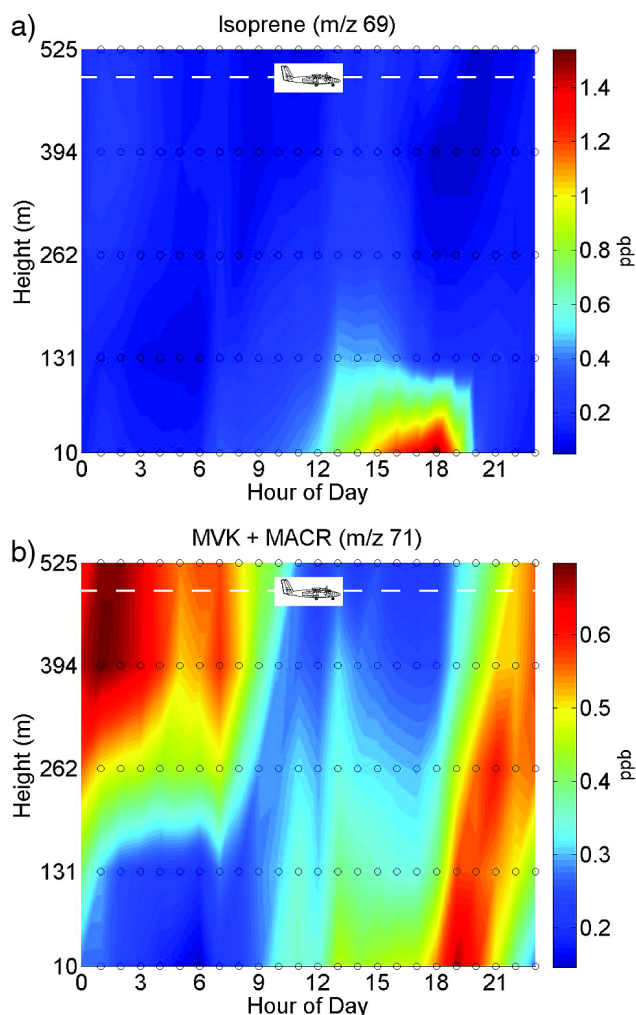


Figure 6. Concentration gradients at Walnut Grove tower for (a) m/z 69 (isoprene) and (b) m/z 71 (dominated by MVK+MAC). The open circles denote the sampling heights. When the aircraft was passing the tower both the tower's top two inlet levels and the aircraft observed very low but non-zero concentrations of isoprene and MVK+MAC. However, the tower data demonstrate that oxidation products of isoprene routinely accumulate at night in the residual layer due to transport from the surrounding foothills where emissions are high. The ground-airborne intercomparison is shown in the Supplement and Supplement Fig. S3.

assessing the true significance of isoprene emissions and its oxidation products for air pollution in areas commonly considered to be dominated by anthropogenic emissions.

3.2.1 Comparison of isoprene fluxes at Tonzi Ranch tower

The aircraft flew over the Tonzi Ranch Tower twice, allowing two snapshot comparisons between the airborne CWT and ground-based relaxed eddy accumulation (REA) flux measurements. It is important to note that the airborne CWT av-

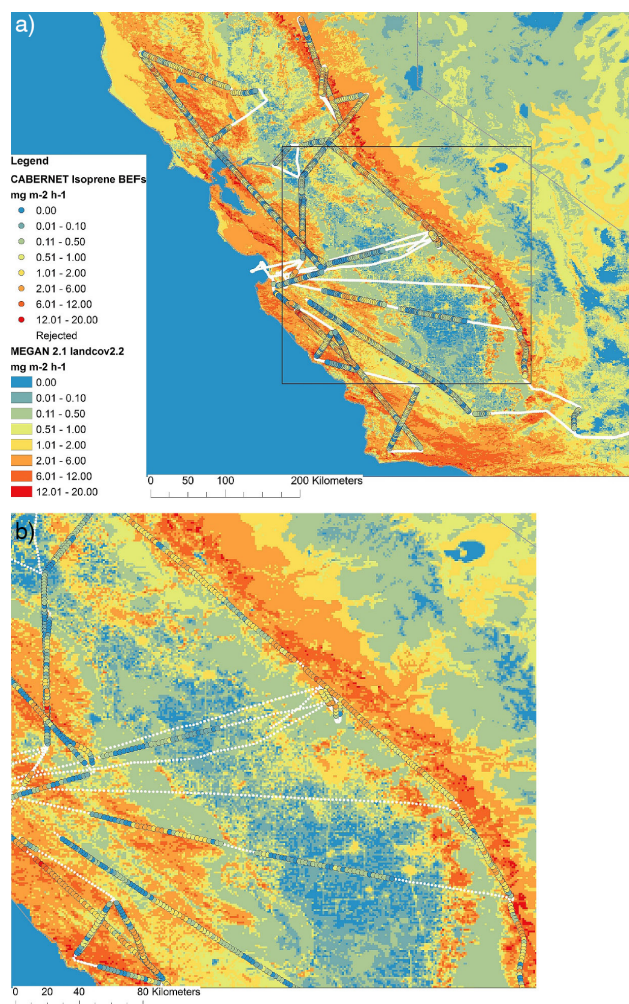


Figure 7. Comparison of airborne BEFs with MEGAN's land cover 2.2 for isoprene (airborne BEFs are subject to additional uncertainties introduced from T , and PAR and the algorithm's activity factor used in normalization). (a) full extent with a rectangle denoting (b) zoomed area. The white dots represent rejected flux data due to flux quality control, aircraft turns, or soundings.

erages over ~ 0.5 min (2 km), while the ground-based REA averages over 30 min, and that the footprints related to each measurement are necessarily quite different, likely do not have the same oak biomass density; and thus the comparison is not expected to be perfect. In the first instance, the half-hourly REA flux was in excellent agreement with the 2 km average wavelet surface flux over the tower (i.e., $0.12 \pm 0.06 \text{ mg m}^{-2} \text{ h}^{-1}$ REA vs. $0.12 \pm 0.06 \text{ mg m}^{-2} \text{ h}^{-1}$ aircraft) while on the returning flight the ground-based flux was 1/3 of the aircraft flux (i.e., $0.26 \pm 0.13 \text{ mg m}^{-2} \text{ h}^{-1}$ REA vs. $0.87 \pm 0.44 \text{ mg m}^{-2} \text{ h}^{-1}$). Interestingly, the next half-hour REA flux was $0.96 \pm 0.48 \text{ mg m}^{-2} \text{ h}^{-1}$, much closer to the aircraft value. This may be due to a shift in wind direction and variability in oak biomass density around the tower but it should also be noted that the uncertainty in a

single REA flux measurement is high and individual values are typically averaged to improve accuracy. These comparisons obviously suffer from significant uncertainties due to different footprints at different altitudes, different temporal coverage, and even temperature/PAR homogeneities. Nevertheless, the comparison provides insight about the variability in measurements at different scales, confirms observations at these scales are in a similar range, and indicates how airplane and tower measurements are complementary. A larger period of overlap in a future campaign is needed for gaining better statistics on such comparisons.

3.2.2 Comparison of isoprene emission factors to MEGAN land cover 2.2

Isoprene emission model estimates are based on basal emission rates, land-cover characteristics, and the changes in emission associated with the environmental parameters temperature and photosynthetically active radiation (PAR). The airborne surface flux normalized for temperature and radiation using the Guenther et al. (2006) activity factor can be used to derive airborne basal emission factors (BEFs) to directly compare to emission factors used by models (e.g., the MEGAN emission factors version 2.2). A spatial comparison is shown in Fig. 7. It needs to be noted that such an approach introduces additional uncertainty from the temperature and PAR data sets and the algorithm used for calculating the activity coefficient, which are much higher than the uncertainty of the measured surface fluxes because of high sensitivity to errors in temperature and PAR. For this reason, in this manuscript we treat this comparison as semi-quantitative, and will explore this in more detail as part of another paper (Misztal et al., 2014) which focuses on using the airborne data to examine the accuracy of several different BVOC emission models, including detailed sensitivity analyses and input data validation. However, the qualitative picture clearly shows the remarkable correspondence of airborne BEFs derived at 2 km spatial resolution with land-cover BEFs at a similar resolution. The transition from the low emitting environment in the Central Valley to highly emitting areas occupied by oak woodlands is clear (as shown earlier in Fig. 1). The most accurate match can be seen, for example, in the central part of the Sierra foothills and on the southern Coastal Range, to the southeast of Monterey Bay and in the oak savannas near San Francisco Bay (Orinda, and Diablo Valley). The BEFs decline to zero over water bodies (e.g., San Francisco Bay, or lakes on the central northern Sierras). There are some areas which do not agree well, for example, in the northeast over the Sierras which are dominated by conifers where airborne BEFs were somewhat lower. On the other hand, the areas where aircraft showed higher BEFs (e.g., beginning of RF8) are most likely related to inaccuracies in the oak land-cover database. For the first time it is now possible to constrain the emission estimates generated by models using direct airborne observations on scales relevant for these

models, and to examine how best to improve modeling approaches including more accurate driving variables and land-cover.

4 Conclusions

We successfully performed airborne eddy covariance flux measurements and mapped out horizontally varying source distributions of isoprene emissions for the dominant oak emitting ecosystems in California. The extensive oak woodlands in California are the most important regional source of isoprene which may be particularly relevant for the photochemistry and air quality near heavily polluted regions of the Central Valley, but also other areas surrounded by substantial areas of oak woodlands including much of the San Francisco Bay Area. We observed high concentrations (up to 8 ppbv) and high surface emissions of isoprene ranging from several to more than $10 \text{ mg m}^{-2} \text{ h}^{-1}$ from the oak woodlands in the foothills of the Sierra Nevada and Coastal Ranges. Consistent with other studies we show that in the Central Valley isoprene emissions are typically undetectably small at aircraft level except for the areas of Eucalyptus trees planted near the highways. However, using the combination of aircraft and tall tower measurements we point out that isoprene chemistry may still play an important role even in those areas where midday isoprene fluxes and concentrations are low, because substantial amounts of isoprene-oxidation products are transported from the surrounding areas which have high emissions and collect in the residual layer at night, mixing down to the surface in the morning. Furthermore, the tower measurements show us that there are at least small isoprene emissions occurring in the valley but the rapid oxidation during the day makes the relatively small emissions from the Central Valley hard to observe at aircraft height. The temperature ranges in California cause changes in the isoprene emissions from relatively low to extremely high due to their strong temperature sensitivity and our flights were performed in early summer season before the highest emissions are expected. The ability of CWT for calculating fluxes at high spatial resolution provides an optimal data set to compare BEFs independent of environmental conditions from measurements with models. The data from this study will be used to assess isoprene emission-factor databases and isoprene emission response to land-cover characteristics predicted for BVOC emission models. The ability to measure direct airborne fluxes over heterogeneous landscapes was needed to improve land-cover descriptions in biogenic emission models. This data set on isoprene fluxes will be particularly useful for evaluating potential model alternatives which will be dealt with in a separate paper to assess isoprene emission models and their driving variable data sets.

The Supplement related to this article is available online at doi:10.5194/acp-14-10631-2014-supplement.

Acknowledgements. We gratefully acknowledge California Air Resources Board (CARB) for funding CABERNET Contract #09-339 and Walnut Grove Contract #11-315, and the CIRPAS team for help in instrument integration. We acknowledge Abhinav Guha (UC Berkeley) for his contributions to the successful campaign. Finally, we would like to thank Andrew Turnipseed (NCAR) and Tiffany Duhl (NCAR) for performing GC analyses of aircraft cartridges, and Steve Shertz (NCAR) for engineering support. NCAR is sponsored by the National Science Foundation. Alex Guenther was partly funded under the Laboratory Directed Research and Development Program at PNNL, a multi-program national laboratory operated by Battelle for the U.S. Department of Energy under Contract DE-AC05-76RL01830. We also acknowledge Prof. Maggi Kelly at GIF, UC Berkeley for suggestions regarding geospatial landcovers. We thank Jeremy Avise and Klaus Scott at California Air Resources Board for collaboration and useful modeling suggestions.

Edited by: A. Hofzumahaus

References

- Apel, E., Riemer, D., Hills, A., Baugh, W., Orlando, J., Faloon, I., Tan, D., Brune, W., Lamb, B., and Westberg, H.: Measurement and interpretation of isoprene fluxes and isoprene, methacrolein, and methyl vinyl ketone mixing ratios at the PROPHET site during the 1998 Intensive, *J. Geophys. Res.*, 107, ACH7-1–ACH7-15, doi:10.1029/2000JD000225, 2002.
- Arey, J., Corchnoy, S. B., and Atkinson, R.: Emission of linalool from Valencia orange blossoms and its observation in ambient air, *Atmos. Environ. A-Gen*, 25, 1377–1381, 1991.
- Arey, J., Crowley, D. E., Crowley, M., Resketo, M., and Lester, J.: Hydrocarbon Emissions from Natural Vegetation in California South-Coast-Air-Basin, *Atmos. Environ.*, 29, 2977–2988, doi:10.1016/1352-2310(95)00137-N, 1995.
- Baker, B., Guenther, A., Greenberg, J., Goldstein, A., and Fall, R.: Canopy fluxes of 2-methyl-3-buten-2-ol over a ponderosa pine forest by relaxed eddy accumulation: Field data and model comparison, *J. Geophys. Res.-Atmos.*, 104, 26107–26114, doi:10.1029/1999jd900749, 1999.
- Baldocchi, D. D.: Assessing the eddy covariance technique for evaluating carbon dioxide exchange rates of ecosystems: past, present and future, *Glob. Change Biol.*, 9, 479–492, 2003.
- Bange, J., Zittel, P., Spiess, T., Uhlenbrock, J., and Beyrich, F.: A new method for the determination of area-averaged turbulent surface fluxes from low-level flights using inverse models, *Bound.-Lay. Meteorol.*, 119, 527–561, doi:10.1007/s10546-005-9040-6, 2006.
- Claussen, M.: Area-Averaging of Surface Fluxes in a Neutrally Stratified, Horizontally Inhomogeneous Atmospheric Boundary-Layer, *Atmos. Environ. A-Gen*, 24, 1349–1360, doi:10.1016/0960-1686(90)90041-K, 1990.
- Desjardins, R. L., Hart, R. L., Macpherson, J. I., Schuepp, P. H., and Verma, S. B.: Aircraft-Based and Tower-Based Fluxes of Carbon-Dioxide, Latent, and Sensible Heat, *J. Geophys. Res.-Atmos.*, 97, 18477–18485, 1992.
- Fares, S., Gentner, D. R., Park, J. H., Ormeno, E., Karlik, J., and Goldstein, A. H.: Biogenic emissions from Citrus species in California, *Atmos. Environ.*, 45, 4557–4568, doi:10.1016/j.atmosenv.2011.05.066, 2011.
- Fares, S., Park, J. H., Gentner, D. R., Weber, R., Ormeno, E., Karlik, J., and Goldstein, A. H.: Seasonal cycles of biogenic volatile organic compound fluxes and concentrations in a California citrus orchard, *Atmos. Chem. Phys.*, 12, 9865–9880, doi:10.5194/acp-12-9865-2012, 2012.
- Fuentes, J. D., and Wang, D.: On the seasonality of isoprene emissions from a mixed temperate forest, *Ecol. Appl.*, 9, 11180–1131, doi:10.2307/2641382, 1999.
- Geron, C., Harley, P., and Guenther, A.: Isoprene emission capacity for US tree species, *Atmos. Environ.*, 35, 3341–3352, 2001.
- Goldstein, A., Hultman, N., Fracheboud, J., Bauer, M., Panek, J., Xu, M., Qi, Y., Guenther, A., and Baugh, W.: Effects of climate variability on the carbon dioxide, water, and sensible heat fluxes above a ponderosa pine plantation in the Sierra Nevada (CA), *Agr. Forest. Meteorol.*, 101, 113–129, 2000.
- Goldstein, A. H., Goulden, M. L., Munger, J. W., Wofsy, S. C., and Geron, C. D.: Seasonal course of isoprene emissions from a mid-latitude deciduous forest, *J. Geophys. Res. Atmos.*, (1984–2012), 103, 31045–31056, 1998.
- Goldstein, A. H. and Schade, G. W.: Quantifying biogenic and anthropogenic contributions to acetone mixing ratios in a rural environment, *Atmos. Environ.*, 34, 4997–5006, doi:10.1016/S1352-2310(00)00321-6, 2000.
- Guenther, A., Karl, T., Harley, P., Wiedinmyer, C., Palmer, P. I., and Geron, C.: Estimates of global terrestrial isoprene emissions using MEGAN (Model of Emissions of Gases and Aerosols from Nature), *Atmos. Chem. Phys.*, 6, 3181–3210, doi:10.5194/acp-6-3181-2006, 2006.
- Guenther, A. B., Jiang, X., Heald, C. L., Sakulyanontvittaya, T., Duhl, T., Emmons, L. K., and Wang, X.: The Model of Emissions of Gases and Aerosols from Nature version 2.1 (MEGAN2.1): an extended and updated framework for modeling biogenic emissions, *Geosci. Model Dev.*, 5, 1471–1492, doi:10.5194/gmd-5-1471-2012, 2012.
- Hegg, D. A., Covert, D. S., Jonsson, H., and Covert, P. A.: Determination of the transmission efficiency of an aircraft aerosol inlet, *Aerosol. Sci. Tech.*, 39, 966–971, doi:10.1080/02786820500377814, 2005.
- Karl, T., Guenther, A., Turnipseed, A., Patton, E. G., and Jardine, K.: Chemical sensing of plant stress at the ecosystem scale, *Biogeosciences*, 5, 1287–1294, doi:10.5194/bg-5-1287-2008, 2008.
- Karl, T., Apel, E., Hodzic, A., Riemer, D. D., Blake, D. R., and Wiedinmyer, C.: Emissions of volatile organic compounds inferred from airborne flux measurements over a megacity, *Atmos. Chem. Phys.*, 9, 271–285, doi:10.5194/acp-9-271-2009, 2009.
- Karl, T., Misztal, P. K., Jonsson, H. H., Shertz, S., Goldstein, A. H., and Guenther, A. B.: Airborne Flux Measurements of BVOCs above Californian Oak Forests: Experimental Investigation of Surface and Entrainment Fluxes, OH Densities, and Damkohler Numbers, *J. Atmos. Sci.*, 70, 3277–3287, doi:10.1175/Jas-D-13-054.1, 2013.
- Karl, T. G., Spirig, C., Rinne, J., Stroud, C., Prevost, P., Greenberg, J., Fall, R., and Guenther, A.: Virtual disjunct eddy covariance measurements of organic compound fluxes from a subalpine forest using proton transfer reaction mass spectrometry, *Atmos. Chem. Phys.*, 2, 279–291, doi:10.5194/acp-2-279-2002, 2002.

- Karlik, J. F. and Winer, A. M.: Measured isoprene emission rates of plants in California landscapes: comparison to estimates from taxonomic relationships, *Atmos. Environ.*, 35, 1123–1131, 2001.
- Karlik, J. F., and McKay, A. H.: Leaf area index, leaf mass density, and allometric relationships derived from harvest of blue oaks in a California oak savanna, USDA Forest Service General Technical Report Number PSW-GTR-184, Albany, CA, 2002.
- Kristensen, L., Mann, J., Oncley, S. P., and Wyngaard, J. C.: How close is close enough when measuring scalar fluxes with displaced sensors?, *J Atmos Ocean Tech*, 14, 814–821, doi:10.1175/1520-0426(1997)014<0814:Hcicew>2.0.Co;2, 1997.
- Kuhn, U., Rottenberger, S., Biesenthal, T., Wolf, A., Schebeske, G., Ciccioli, P., Brancaleoni, E., Frattoni, M., Tavares, T., and Kesselmeier, J.: Isoprene and monoterpene emissions of Amazonian tree species during the wet season: Direct and indirect investigations on controlling environmental functions, *J. Geophys. Res.*, 107, 8071, doi:10.1029/2001JD000978, 2002.
- Kurpius, M. R., and Goldstein, A. H.: Gas-phase chemistry dominates O₃ loss to a forest, implying a source of aerosols and hydroxyl radicals to the atmosphere, *Geophys. Res. Lett.*, 30, 1371 doi:10.1029/2002gl016785, 2003.
- Lamb, B., Westberg, H., and Allwine, G.: Isoprene Emission Fluxes Determined by an Atmospheric Tracer Technique, *Atmos. Environ.*, 20, 1–8, doi:10.1016/0004-6981(86)90201-5, 1986.
- Langford, B., Misztal, P. K., Nemitz, E., Davison, B., Helfter, C., Pugh, T. A. M., MacKenzie, A. R., Lim, S. F., and Hewitt, C. N.: Fluxes and concentrations of volatile organic compounds from a South-East Asian tropical rainforest, *Atmos. Chem. Phys.*, 10, 8391–8412, doi:10.5194/acp-10-8391-2010, 2010.
- Lenschow, D. H., Delany, A. C., Stankov, B. B., and Stedman, D. H.: Airborne Measurements of the Vertical Flux of Ozone in the Boundary-Layer, *Bound.-Lay. Meteorol.*, 19, 249–265, doi:10.1007/Bf00117223, 1980.
- Lenschow, D. H., Pearson, R., and Stankov, B. B.: Estimating the ozone budget in the boundary-layer by use of aircraft measurements of ozone eddy flux and mean concentration, *J. Geophys. Res.-Oc. Atm.*, 86, 7291–7297, 1981.
- Lenschow, D. H.: Probing the Atmospheric Boundary Layer, Probing the Atmospheric Boundary Layer, American Meteorological Society, Boston, MA, 1986.
- Loreto, F., and Sharkey, T. D.: A gas-exchange study of photosynthesis and isoprene emission in *Quercus rubra* L, *Planta*, 182, 523–531, 1990.
- Mahrt, L.: Surface heterogeneity and vertical structure of the boundary layer, *Bound.-Lay. Meteorol.*, 96, 33–62, doi:10.1023/A:1002482332477, 2000.
- Mann, J. and Lenschow, D. H.: Errors in Airborne Flux Measurements, *J. Geophys. Res.-Atmos.*, 99, 14519–14526, doi:10.1029/94jd00737, 1994.
- Mason, P. J.: The Formation of Areal-averaged Roughness Lengths, *Q. J. Roy. Meteor. Soc.*, 114, 399–420, doi:10.1002/qj.49711448007, 1988.
- Mauder, M., Desjardins, R. L., and MacPherson, I.: Scale analysis of airborne flux measurements over heterogeneous terrain in a boreal ecosystem, *J. Geophys. Res.-Atmos.*, 112, D13112, doi:10.1029/2006jd008133, 2007.
- Metzger, S., Junkermann, W., Mauder, M., Butterbach-Bahl, K., Trancón y Widemann, B., Neidl, F., Schäfer, K., Wieneke, S., Zheng, X. H., Schmid, H. P., and Foken, T.: Spatially explicit regionalization of airborne flux measurements using environmental response functions, *Biogeosciences*, 10, 2193–2217, doi:10.5194/bg-10-2193-2013, 2013.
- Misztal, P. K., Avise, J., Karl, T., Scott, K., Weber, R., Jonsson, H. H., Guenther, A. B., and Goldstein, A. H.: Evaluation of regional isoprene emission estimates in California based on direct airborne flux measurements, in preparation for ES&T, 2014.
- Moore, C.: Frequency response corrections for eddy correlation systems, *Bound.-Lay. Meteorol.*, 37, 17–35, 1986.
- Nordbo, A., and Katul, G.: A Wavelet-Based Correction Method for Eddy-Covariance High-Frequency Losses in Scalar Concentration Measurements, *Bound.-Lay. Meteorol.*, 146, 81–102, doi:10.1007/s10546-012-9759-9, 2013.
- Panofsky, H. A. and Dutton, J. A.: Atmospheric turbulence: models and methods for engineering applications, Wiley, New York, 1984.
- Park, J.-H., Goldstein, A. H., Timkovsky, J., Fares, S., Weber, R., Karlik, J., and Holzinger, R.: Active Atmosphere-Ecosystem Exchange of the Vast Majority of Detected Volatile Organic Compounds, *Science*, 341, 643–647, doi:10.1126/science.1235053, 2013.
- Pattey, E., Strachan, I., Desjardins, R., and Massheder, J.: Measuring nighttime CO₂ flux over terrestrial ecosystems using eddy covariance and nocturnal boundary layer methods, *Agr. Forest. Meteorol.*, 113, 145–158, 2002.
- Pierce, T., Geron, C., Bender, L., Dennis, R., Tonnesen, G., and Guenther, A.: Influence of increased isoprene emissions on regional ozone modeling, *J. Geophys. Res.-Atmos.*, 103, 25611–25629, doi:10.1029/98jd01804, 1998.
- Rasmussen, R. A.: Isoprene: Identified as a forest-type emission to the atmosphere, *Environ. Sci. Technol.*, 4, 667–671, 1970.
- Raupach, M. R., and Finnigan, J. J.: Scale Issues in Bound.-Lay. Meteorol. – Surface-Energy Balances in Heterogeneous Terrain, *Hydrol. Proc.*, 9, 589–612, doi:10.1002/hyp.3360090509, 1995.
- Reid, J. S., Jonsson, H. H., Smith, M. H., and Smirnov, A.: Evolution of the vertical profile and flux of large sea-salt particles in a coastal zone, *J. Geophys. Res.-Atmos.*, 106, 12039–12053, doi:10.1029/2000jd900848, 2001.
- Rinne, H., Guenther, A., Greenberg, J., and Harley, P.: Isoprene and monoterpene fluxes measured above Amazonian rainforest and their dependence on light and temperature, *Atmos. Environ.*, 36, 2421–2426, 2002.
- Rowe, M. D., Fairall, C. W., and Perlinger, J. A.: Chemical sensor resolution requirements for near-surface measurements of turbulent fluxes, *Atmos. Chem. Phys.*, 11, 5263–5275, doi:10.5194/acp-11-5263-2011, 2011.
- Schade, G. W., Goldstein, A. H., and Lamanna, M. S.: Are monoterpene emissions influenced by humidity?, *Geophys. Res. Lett.*, 26, 2187–2190, doi:10.1029/1999gl900444, 1999.
- Schade, G. W., Goldstein, A. H., Gray, D. W., and Lerdau, M. T.: Canopy and leaf level 2-methyl-3-buten-2-ol fluxes from a ponderosa pine plantation, *Atmos. Environ.*, 34, 3535–3544, doi:10.1016/S1352-2310(00)00120-5, 2000.
- Schade, G. W., and Goldstein, A. H.: Fluxes of oxygenated volatile organic compounds from a ponderosa pine plantation, *J. Geophys. Res.-Atmos.*, 106, 3111–3123, doi:10.1029/2000jd900592, 2001.
- Scott, K. I. and Benjamin, M. T.: Development of a biogenic volatile organic compounds emission inventory for the

- SCOS97-NARSTO domain, *Atmos. Environ.*, 37, S39–S49, doi:10.1016/S1352-2310(03)00381-9, 2003.
- Serca, D., Guenther, A., Klinger, L., Vierling, L., Harley, P., Druihet, A., Greenberg, J., Baker, B., Baugh, W., Bouka-Biona, C., and Loemba-Ndembu, J.: EXPRESSO flux measurements at upland and lowland Congo tropical forest site, *Tellus B*, 53, 220–234, doi:10.1034/j.1600-0889.2001.01237.x, 2001.
- Sharkey, T. D., Singaas, E. L., Lerdau, M. T., and Geron, C. D.: Weather effects on isoprene emission capacity and applications in emissions algorithms, *Ecol. Appl.*, 9, 1132–1137, 1999.
- Steiner, A. L., Pressley, S. N., Botros, A., Jones, E., Chung, S. H., and Edburg, S. L.: Analysis of coherent structures and atmosphere-canopy coupling strength during the CABINEX field campaign, *Atmos. Chem. Phys.*, 11, 11921–11936, doi:10.5194/acp-11-11921-2011, 2011.
- Steiner, A. L., Tonse, S., Cohen, R. C., Goldstein, A. H., and Harley, R. A.: Influence of future climate and emissions on regional air quality in California, *J. Geophys. Res. Atmos.* (1984–2012), 111, D18303, doi:10.1029/2005JD006935, 2006.
- Stoy, P. C., Richardson, A. D., Baldocchi, D. D., Katul, G. G., Stanovick, J., Mahecha, M. D., Reichstein, M., Detto, M., Law, B. E., Wohlfahrt, G., Arriga, N., Campos, J., McCaughey, J. H., Montagnani, L., Paw U, K. T., Sevanto, S., and Williams, M.: Biosphere-atmosphere exchange of CO₂ in relation to climate: a cross-biome analysis across multiple time scales, *Biogeosciences*, 6, 2297–2312, doi:10.5194/bg-6-2297-2009, 2009.
- Thomas, C. and Foken, T.: Detection of long-term coherent exchange over spruce forest using wavelet analysis, *Theor. Appl. Climatol.*, 80, 91–104, 2005.
- Thomas, C., and Foken, T.: Flux contribution of coherent structures and its implications for the exchange of energy and matter in a tall spruce canopy, *Bound.-Lay. Meteorol.*, 123, 317–337, doi:10.1007/s10546-006-9144-7, 2007.
- Torrence, C. and Compo, G. P.: A practical guide to wavelet analysis, *B Am Meteorol Soc*, 79, 61–78, 1998.
- Vargas, R., Detto, M., Baldocchi, D. D., and Allen, M. F.: Multi-scale analysis of temporal variability of soil CO₂ production as influenced by weather and vegetation, *Glob. Change Biol.*, 16, 1589–1605, 2010.
- Weil, J. C. and Horst, T. W.: Footprint Estimates for Atmospheric Flux Measurements in the Convective Boundary-Layer, *Precipitation Scavenging and Atmosphere-Surface Exchange*, 1–3, 717–728, 1992.
- Westberg, H., Lamb, B., Hafer, R., Hills, A., Shepson, P., and Vogel, C.: Measurement of isoprene fluxes at the PROPHET site, *J. Geophys. Res. Atmos.* (1984–2012), 106, 24347–24358, 2001.
- Winer, A. M., Arey, J., Atkinson, R., Aschmann, S. M., Long, W. D., Morrison, C. L., and Olszyk, D. M.: Emission Rates of Organics from Vegetation in California Central Valley, *Atmos. Environ. A-Gen*, 26, 2647–2659, doi:10.1016/0960-1686(92)90116-3, 1992.
- Wood, N., and Mason, P.: The Influence of Static Stability on the Effective Roughness Lengths for Momentum and Heat-Transfer, *Q. J. Roy. Meteor. Soc.*, 117, 1025–1056, doi:10.1002/qj.49711750108, 1991.
- Wyngaard, J. C. and Brost, R. A.: Top-down and bottom-up diffusion of a scalar in the convective boundary layer, *J. Atmos. Sci.*, 41, 102–112, 1984.